Simulation of Mass Sensor Based on Luminescence of Micro/Nano Electromechanical Resonator

Lijie Li, *Senior Member, IEEE*

***Abstract*—We report a novel mass sensor based on detecting the luminescence from micro/nano electromechanical resonators. Multi-physics simulation has been conducted to elucidate this concept. It is found that the added mass affects both the resonant frequency and oscillating amplitude of the mechanical resonator. However we mainly use the change of oscillating amplitude to detect the added mass by observing varied optical intensity. For the device simulated, the sensitivity ($(\Delta f/f_0)/\delta m$ per microgram) is 2% μg^{-1} if using frequency measurement through electronic circuits, while the sensitivity ($(\Delta I_L/I_0)/\delta m$ per microgram) is 377% μg^{-1} using amplitude measurement through the proposed optical method.**

***Index Terms*—Mass sensor, Luminescence, Piezoelectric.**

I. Introduction

RESEARCH on mass sensors made of micro/nano resonators has become a major subject due to their ability of achieving high sensitivity [1] [2]. The working principle of this type of sensors is detecting the mass of particles landed on the resonator through monitoring the variation of its resonant frequency [3] [4]. There have been two dominant readout methods, namely electronic and optical readout. For the electronic readout, requency measurement circuits are needed to extract the frequency change of the resonator [5]. For the optical readout mechanism, quite often a precisely aligned optical setup is required, i.e. shining an optical beam onto the resonator surface and collecting the reflected optical signal [6]. For the latter, the smoothness and roughness of the sensor surface are critical as the reflected optical signal can be deflected or weakened by the increasing roughness due to landed particles. It is worth noting that the optical method is able to avoid the heating effect and energy loss caused by electronic circuits [7]. Our approach of using luminescence of the resonator itself addresses the above issues, as the frequency measurement circuits are not necessary, and the surface properties of the mechanical structure do not cause any significant degradation of the luminescence. The proposed sensing mechanism is described as follows: As the cantilever vibrates, piezoelectric charges are generated from the mechanical strain and stress. These charges enhance the intensity of the luminescence according to the stimulated emission theory. When particles land on the cantilever, both the amplitude and frequency of the oscillation are affected, of which the amplitude change induces the variation of generated piezoelectric charges. This is detected by the intensity of photoluminescence. A systematic multi-physics simulation is presented in this letter to demonstrate this hypothesis.

L. Li is with the college of engineering, Swansea University, Swansea, UK, SA1 8EN. Email: l.li@swansea.ac.uk

The author would like to thank Swansea University for support.
Manuscript received December 2016

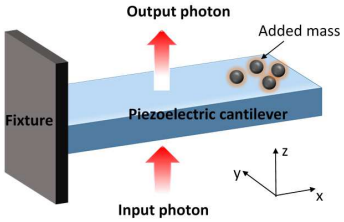

Fig. 1. Schematic of the new sensing mechanism. The piezoelectric cantilever produces varied luminescence subjecting to deflections, which are affected by the loaded mass.

II. Theory

The proposed sensor device is structured to a cantilever shape with one end fixed and the other suspended (Figure 1). A piezoelectric material, zinc oxide (ZnO) is chosen to form the cantilever, as it exhibits photoluminescence band of (300nm-400nm) [8] as well as having piezoelectricity property [9]. For this particular material we have chosen to simulate, visible luminescence was demonstrated in [10] [11]. Measurement of the output light intensity can be achieved by a spectrometer or CCD, through which piezoelectric induced intensity change was observed in a prior reference [11]. There are two known parameters of the material affecting the stimulated luminescence, one is the charge density, the other is the bandgap of the material. For large dimension bulk devices (in micro/millimetre range, such as thin film), the charge density factor dominates. For nanoscale devices (nanowires, nanosheet), strain induced bandgap variation becomes an important factor. For the micrometer sized device described below, only the charge density factor needs to be considered.

The length L, width w, and thickness g of the cantilever are designated as 2 mm, 0.2 mm, and 20 μm in the numerical modelling. ZnO is chosen as the piezoelectric material with density $\rho = 5606\ kg/m^3$, and Young's modulus $Y = 100\ GPa$ [12]. The dynamic motion of the cantilever can be described based on Euler−Bernoulli beam theory, simplified to a mass-spring-damper system [13]

$$m_c\frac{d^2z}{dt^2} + b\frac{dz}{dt} + k_1 z + k_2 z^3 = Acos(\omega t) \qquad (1)$$

where m_c, b, k_1, k_2 are total effective mass $(\frac{33}{140})Lwg\rho$, damping coefficient, linear stiffness, and nonlinear stiffness

respectively. $z(t)$ denotes the tip displacement. The first derivative of the z with respect to the time t represents the velocity, and the second derivative denotes the acceleration. $A = m_t * a$ (m_t is the total mass that is the sum of m_c and the added mass, and a is the applied acceleration) is the amplitude of the external periodic driving force, and ω is the driving frequency. When $\omega = \omega_0$ (ω_0 being the natural frequency of the cantilever $\omega_0 = \sqrt{\frac{k_1}{m_c}}$, here we only analyse the fundamental resonance), the deflection of the cantilever reaches its maximum. We set the driving frequency same as the natural frequency of the cantilever for each added mass to ensure an optimal energy transfer from the excitation to the cantilever. The amplitude of the external driving acceleration a is kept constant throughout the simulation process. In the small deflection region (simulated maximum tip deflection is around 0.02 nm, while the thickness of the cantilever is 20 μm), the curvature can be approximated at any point of the beam by $\frac{1}{r} = \frac{\tau}{YI}$, where τ is the mechanical moment applied on the beam, and I is the moment of inertia. The tip displacement can be expressed as $z = \frac{\tau L^2}{2YI}$, hence the curvature at a time t is derived as

$$\frac{1}{r(t)} = \frac{2z(t)}{L^2} \tag{2}$$

where $r(t)$ is the radius of the curvature. The axial strain on the surface of the piezoelectric layer along the x-axis can be obtained in terms of the curvature and tip deflection [13]

$$\varepsilon_x(t) = \frac{g}{2r(t)} \tag{3}$$

The axial stress σ on the piezoelectric surface is derived through the stress-strain relation, that is $\sigma_x(t) = Y\varepsilon_x(t)$. The piezoelectric constitutive equations connect four field variables stress components Σ, strain components S, electric field components E, and the electric displacement components D, which can be described as $\begin{bmatrix} S \\ D \end{bmatrix} = \begin{bmatrix} s^E & d^t \\ d & \varepsilon^T \end{bmatrix} \begin{bmatrix} \Sigma \\ E \end{bmatrix}$ [14] [15]. The generated electric displacement D from the mechanical stress Σ can be expressed as $D = d\Sigma$ assuming no external electric field is applied to the cantilever, where d represents the piezoelectric constant. The electrical charges (here only electrons either on top or bottom surface are considered) generated from a tip deflection $z(t)$ can be obtained as

$$Q(t) = wLd_{31}\sigma_x(t) = \frac{wd_{31}Yg}{L}z(t) \tag{4}$$

where d_{31} is the piezoelectric constant, relating the strain in the '1' direction (x-axis) to a generated field along the '3' direction (z-axis). In the simulation, we take d_{31}=−3.3 pC/N. An upward deflection ($z > 0$) corresponds to a compressive stress on the top surface, therefore inducing negative charges.

Generated charges can be expressed as carrier density of the cantilever (divided by the volume of the cantilever). To simplify the problem for demonstration purpose, the material is assumed intrinsic and there is no internal screening effect.

The chemical potential is required for arriving at Fermi-Dirac distributions of electrons in both the conduction band and valence band, in order to calculate the stimulated emission rate. The chemical potentials are calculated using the iteration/self-consistent method [16] based on the expression of the carrier density n [17]

$$\begin{aligned} n &= \int_0^\infty D_3(\mathcal{E}) f_0(\mathcal{E}) d\mathcal{E} \\ &= \frac{1}{2\pi^2}(\frac{2m^*}{\hbar^2})^{3/2} \int_0^\infty \frac{\mathcal{E}^{1/2}}{\exp(\frac{\mathcal{E}-\mu}{k_B T}) + 1} d\mathcal{E} \end{aligned} \tag{5}$$

where $D_3(\mathcal{E})$ represents the density of state for 3-dimensional bulk materials measuring numbers of electron states per unit energy interval, which takes the form of $\frac{1}{2\pi^2}(\frac{2m^*}{\hbar^2})^{3/2}\mathcal{E}^{1/2}$ [18], where $\hbar$ is the reduced Planck's constant ($1.05 \times 10^{-34} Js$), m^* is the effective mass of electron $m_e = 0.24m_0$ or hole $m_h = 0.59m_0$, where m_0 is the bare electron mass $m_0 = 9.11 \times 10^{-31} Kg$. n is the carrier density, which is varying upon deflection of the piezoelectric cantilever. $f_0(\mathcal{E})$ is the Fermi distribution of electrons $\frac{1}{\exp(\frac{\mathcal{E}-\mu}{k_B T})+1}$, where $\mathcal{E}$ is the electron energy, μ stands for the chemical potential, k_B is the Boltzmann constant ($8.62 \times 10^{-5} eV/K^{-1}$), and T denotes the temperature.

The calculated chemical potentials are then used in the equation for simulating the total stimulated emission based on Fermi Golden rule, which is

$$\begin{aligned} R_s =& \frac{2\pi}{\hbar} \frac{(\hbar\omega)^2 n_r^3}{\pi^2 \hbar^3 c^3} \frac{1}{\exp(\frac{\hbar\omega}{k_B T}) - 1} |M_{fi}|^2 \\ & \times \frac{1}{2\pi^2}(\frac{2m_r}{\hbar})^{3/2} (\hbar\omega - \mathcal{E}_g)^{1/2} f_c(1 - f_v) \end{aligned} \tag{6}$$

where M_{fi} is the perturbing potential during the electron transition from initial to final state, and $|M_{fi}|^2$ is the squared matrix element coupling the initial and final states. For most of semiconductor materials, $|M_{fi}|^2$ can be treated as a constant. $\frac{1}{\exp(\frac{\hbar\omega}{k_B T})-1}$ is the Bose-Einstein distribution for photons, and $\frac{1}{2\pi^2}(\frac{2m_r}{\hbar})^{3/2}(\hbar\omega - \mathcal{E}_g)^{1/2}$ is the 3D density of electron states. Where n_r is the refractive index in the medium, $\hbar\omega$ denotes the photon energy, c is the speed of light in vacuum, and m_r is the combined reduced mass ($\frac{1}{m_r} = \frac{1}{m_e} + \frac{1}{m_h}$). f_c and f_v give Fermi-Dirac distributions in conduction and valence band respectively. As the effective electron mass and hole mass are slightly different, the chemical potential μ_c deviates gradually from the μ_h for large carrier densities. Equation (6) can be written to a simple form by grouping all the constants, which is

$$R_s = C \frac{(\hbar\omega)^2}{\exp(\frac{\hbar\omega}{k_B T}) - 1} (\hbar\omega - \mathcal{E}_g)^{1/2} f_c(1 - f_v) \tag{7}$$

where $C = \frac{2\sqrt{2} n_r^3 |M_{fi}|^2 m_r^{3/2}}{\pi^3 c^3 \hbar^{11/2}}$. Simulation is conducted in the next section according to the theory and method described above.

III. Numerical simulation

Results have been obtained from the numerical simulation. The intensity of incident photon is kept constant. It is shown in the Figure 2 that the resonant frequency reduces from 3444

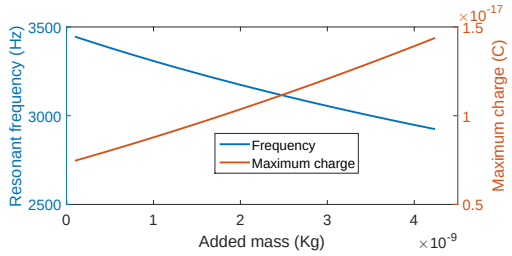

Fig. 2. Simulated resonant frequency and charge generation of the piezoelectric resonator vs. added mass.

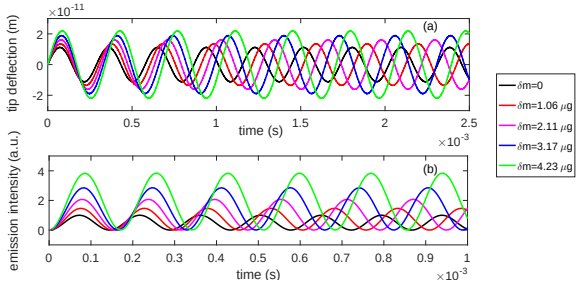

Fig. 3. (a) Tip displacement in time domain for various values of added mass. (b) Stimulated emission intensity in time domain when resonator is oscillating for various values of added mass. The amplitude of the periodic external force and the incident photon energy are constant.

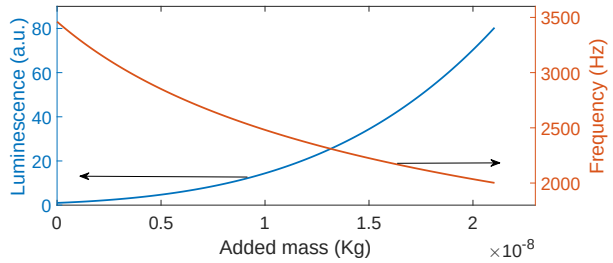

Fig. 4. Resonant frequency and emission intensity vs. added mass.

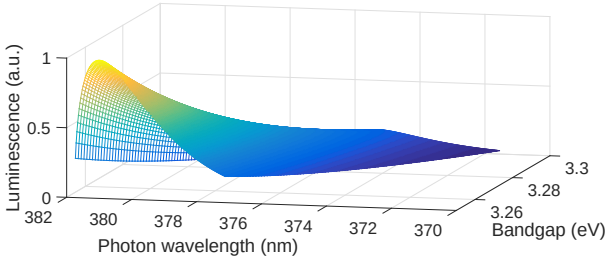

Fig. 5. Spectrum and intensity of the stimulated emission for various bandgaps for nanoscale resonators. The charge density is fixed at $1\times10^{20}\ m^{-3}$ without considering piezoelectric effect.

Hz to 2925 Hz, and the maximum generated charge increases from 7.467×10^{-18} C to 1.436×10^{-17} C, when the value of added mass increases from 0.11 μg to 4.2 μg. Figure 3a shows the tip deflection of this piezoelectric cantilever for different values of mass landed. It is seen that the added mass causes the deflection amplitude to increase and resonant frequency to decrease. Figure 3b displays the results on the intensity of the luminescence in relation to the added mass, where the intensity increases more significantly than the reduction of resonant frequency. Figure 4 shows more detailed results relating the emission intensity and the added mass. It is shown when the added mass value increases around 200 times, the emission intensity I_L is enhanced around 80 times corresponding to a sensitivity ($(\Delta I_L/I_0)/\delta m$ per microgram) of 377% μg^{-1}, whereas the resonant frequency f is reduced to around 42% of its original value, corresponding to a sensitivity ($(\Delta f/f_0)/\delta m$ per microgram) of 2% μg^{-1}. To calculate the sensitivity, the emission intensity of no added mass has been calculated ($I_0 = 1\ a.u.$). When a mass is added ($\delta m = 21\mu g$), the luminescence is calculated to be $I_L = 80.3\ a.u.$. So the resolution ($\frac{\Delta I_L/I_0}{\delta m} = \frac{|I_L - I_0|/(I_0)}{\delta m}$ per microgram) is obtained. Same procedure is used to arrive at the frequency resolution.

The device proposed in this work has a larger dimension of 2 mm $\times$ 0.2 mm $\times$ 20 μm, therefore the bandgap is immune to the axial strain. The emission is mainly dependent on increasing charge density due to piezoelectric effect. From the simulation, the added mass leads to the increase of the oscillation amplitude, inducing more piezoelectric charges, subsequently increasing the charge density.

For nanoscale features such as ZnO nanowires, their luminescence spectrum and intensity vary upon uniaxial strain along c-axis direction and dimension along the radial direction according to reference [19] [11], elucidated by the surface effect and quantum confinement. Nanowires with smaller diameters have wider bandgaps than those with larger diameters due to increased surface-volume ratios, uniaxial tensile strain shifts the bandgap downward. The impact due to strain is more pronounced for nanowires with diameters smaller than 200 nm. There are other compound semiconductor nanofeatures exhibit strain dependent emissions such as GaAs nanowire [20], MoS_2 nanosheet [21]. There is no report on this effect for ZnO bulk or films.

Additional analysis has been conducted in this work for revealing the relation of bandgap and emission spectrum for the nanoscale resonators, in which the charge density remains as a constant. It is seen from the Figure 5 that as the bandgap decrease from 3.3 eV to 3.25 eV, the amplitude of the peak emission shifts upward by around 6.6 times, with the wavelength of the peak emission increases from 375 nm to 381 nm.

IV. Conclusion

A novel mass sensor based on detecting variation of stimulated emission of the micro/nano resonators has been analysed using the coupled electromechanical-quantum mechanics theory. The results show that the change of emission intensity subjecting to the added mass is more pronounced than the change of the mechanical resonant frequency.

References

[1] J. Chaste, A. Eichler, J. Moser, G. Ceballos, R. Rurali, and A. Bachtold, "A nanomechanical mass sensor with yoctogram resolution," *Nat Nano*, vol. 7, no. 5, pp. 301–304, 2012, doi: 10.1038/nnano.2012.42.

[2] A. K. Naik, M. S. Hanay, W. K. Hiebert, X. L. Feng, and M. L. Roukes, "Towards single-molecule nanomechanical mass spectrometry," *Nat Nano*, vol. 4, no. 7, pp. 445–450, 2009, doi: 10.1038/nnano.2009.152.

[3] L. Jin and L. Li, "A novel mass sensor based on nanomechanical transistor," *IEEE Electron Device Letters*, vol. 36, no. 1, pp. 68–70, 2015, doi: 10.1109/LED.2014.2374693.

[4] L. Li, "Recent development of micromachined biosensors," *IEEE Sensors Journal*, vol. 11, no. 2, pp. 305–311, 2011, doi: 10.1109/JSEN.2010.2063424.

[5] S. Hafizi-Moori and E. Cretu, "Weakly-coupled resonators in capacitive readout circuits," *IEEE Transactions on Circuits and Systems I: Regular Papers*, vol. 62, no. 2, pp. 337–346, Feb 2015, doi: 10.1109/TCSI.2014.2365331.

[6] V. P. Adiga, R. De Alba, I. R. Storch, P. A. Yu, B. Ilic, R. A. Barton, S. Lee, J. Hone, P. L. McEuen, J. M. Parpia, and H. G. Craighead, "Simultaneous electrical and optical readout of graphene-coated high q silicon nitride resonators," *Applied Physics Letters*, vol. 103, no. 14, p. 143103, 2013, doi: 10.1063/1.4823457.

[7] J.-J. Li and K.-D. Zhu, "All-optical mass sensing with coupled mechanical resonator systems," *Physics Reports*, vol. 525, no. 3, pp. 223 – 254, 2013, doi: 10.1016/j.physrep.2012.11.003.

[8] J. Ji, A. M. Colosimo, W. Anwand, L. A. Boatner, A. Wagner, P. S. Stepanov, T. T. Trinh, M. O. Liedke, R. Krause-Rehberg, T. E. Cowan, and F. A. Selim, "Zno luminescence and scintillation studied via photoexcitation, x-ray excitation, and gamma-induced positron spectroscopy," *Scientific Reports*, vol. 6, p. 31238, 2016, doi: 10.1038/srep31238.

[9] L. B. Francesca, D. Timothy, D. Anuja, A. W. Richard, S. Suman-Lata, and K.-N. Sohini, "Vertically aligned zinc oxide nanowires electrodeposited within porous polycarbonate templates for vibrational energy harvesting," *Nanotechnology*, vol. 27, no. 28, p. 28LT02, 2016, doi: 10.1088/0957-4484/27/28/28LT02.

[10] J. Liu, S. Lee, Y. H. Ahn, J.-Y. Park, and K. H. Koh, "Tailoring the visible photoluminescence of mass-produced zno nanowires," *Journal of Physics D: Applied Physics*, vol. 42, no. 9, p. 095401, 2009, doi: 10.1088/0022-3727/42/9/095401.

[11] C. Pan, L. Dong, G. Zhu, S. Niu, R. Yu, Q. Yang, Y. Liu, and Z. L. Wang, "High-resolution electroluminescent imaging of pressure distribution using a piezoelectric nanowire led array," *Nat Photon*, vol. 7, no. 9, pp. 752–758, 2013, doi: 10.1038/NPHOTON.2013.191.

[12] M. Lucas, W. Mai, R. Yang, Z. L. Wang, and E. Riedo, "Aspect ratio dependence of the elastic properties of zno nanobelts," *Nano Letters*, vol. 7, no. 5, pp. 1314–1317, 2007, doi: 10.1021/nl070310g.

[13] L. Jin, J. Mei, and L. Li, "Analysis of intrinsic localised mode for a new energy harvesting cantilever array," *European Physical Journal Applied Physics*, vol. 66, p. 10902, 2014, doi: 10.1051/epjap/2014130565.

[14] S. O. R. Moheimani and A. J. Fleming, *Piezoelectric Transducers for Vibration Control and Damping*. Springer London, 2006.

[15] A. Erturk and D. J. Inman, *Piezoelectric Energy Harvesting*. John Wiley and Sons, Inc., West Sussex, UK, 2011.

[16] Y. Zhang and L. Li, "Piezophototronic effect enhanced luminescence of zinc oxide nanowires," *Nano Energy*, vol. 22, pp. 533 – 538, 2016, doi: 10.1016/j.nanoen.2016.02.039.

[17] A. F. J. Levi, *Applied Quantum Mechanics*. Cambridge University Press, Cambridge, UK, 2006.

[18] S. M. Sze and K. K. Ng, *Physics of Semiconductor Devices*. John Wiley and Sons, Inc., Hoboken, New Jersey, 2007.

[19] B. Wei, K. Zheng, Y. Ji, Y. Zhang, Z. Zhang, and X. Han, "Size-dependent bandgap modulation of zno nanowires by tensile strain," *Nano Letters*, vol. 12, no. 9, pp. 4595–4599, 2012, doi: 10.1021/nl301897q.

[20] G. Signorello, S. Karg, M. T. Bjrk, B. Gotsmann, and H. Riel, "Tuning the light emission from gaas nanowires over 290 mev with uniaxial strain," *Nano Letters*, vol. 13, no. 3, pp. 917–924, 2013, doi: 10.1021/nl303694c.

[21] Y. Y. Hui, X. Liu, W. Jie, N. Y. Chan, J. Hao, Y.-T. Hsu, L.-J. Li, W. Guo, and S. P. Lau, "Exceptional tunability of band energy in a compressively strained trilayer mos2 sheet," *ACS Nano*, vol. 7, no. 8, pp. 7126–7131, 2013, doi: 10.1021/nn4024834.